Heliyon 10 (2024) e28993

Contents lists available at ScienceDirect

Heliyon

journal homepage: www.cell.com/heliyon

Research article

Non-similar bioconvective analysis of magnetized hybrid nanofluid ($Ag + TiO_2$) flow over exponential stretching surface

Jifeng Cui [a,*], Haseena [b], Umer Farooq [c], Ahmed Jan [b], Muzamil Hussain [d]

[a] College of Science, Inner Mongolia University of Technology, Hohhot 010051, China
[b] Department of Mathematics, COMSATS University Islamabad, Park Road Chak Shahzad, Islamabad 44000, Pakistan
[c] College of Mathematical Science, Harbin Engineering University, Harbin city 150001, Heilongjiang, China
[d] Department of Mathematics, University of the Poonch Rawalakot, Rawalakot 123350, Pakistan

ARTICLE INFO

Keywords:
Local non-similarity
Exponential stretching sheet
Magnetohydrodynamic (MHD)
Hybrid nanofluid
Bioconvection
bvp4c

ABSTRACT

Scientists have studied fluid flow over a stretching sheet to explore its potential applications in industries. This study investigates the exponential stretching flow of a bioconvective magnetohydrodynamic (MHD) hybrid nanofluid in porous medium taking into consideration thermal radiations, heat generation, chemical reaction, porosity, and dissipation. Moreover, microorganisms are present in the fluid, so the fluid is more stable, which is crucial in biotechnology, biomicrosystems, and bio-nano coolant systems. Silver and titanium dioxide in a water-based medium are the prototypical nanoparticles. The present study involves a transformation of the governing system into a set of dimensionless, coupled and nonlinear partial differential equations (PDEs) using nonsimilar techniques. The local non-similarity (LNS) technique is used to truncate these equations to ordinary differential equations (ODEs). This technique is also used to estimate transformed equations numerically until the second level of truncation takes place via the bvp4c algorithm, which is a built-in MATLAB solver. Furthermore, tables are provided that presents the drag coefficients, Nusselt numbers, Sherwood numbers, and densities of motile microorganisms. Results show a negative correlation between the velocity and the magnetic field parameter as well as the porosity parameter, as evidenced by a decrease in velocity corresponds to rises in these parameters. The temperature distribution exhibits a positive correlation with the rising values of both radiation parameter and Eckert number. The concentration profiles also exhibit a negative correlation with the increasing values of Lewis and bioconvection Lewis number, chemical reaction parameter, Peclet number and the differences in microbial concentration. This study will improve the future research on hybrid nanofluid regarding industrial applications. There haven't been any previous publications that have investigated the use of this model with the local non-similarity method. The main objective of this article is to enhance the heat transfer performance in a hybrid nanofluid.

* Corresponding author.
E-mail addresses: cjf@imut.edu.cn (J. Cui), umer_farooq@hrbeu.edu.cn (U. Farooq).

https://doi.org/10.1016/j.heliyon.2024.e28993
Received 24 July 2023; Received in revised form 27 March 2024; Accepted 27 March 2024

Available online 2 April 2024

Nomenclature

u, v	Velocity components ..... ms^{-1}	ν	Fluid's kinematic viscosity ..... $m^2 s^{-1}$
T	Fluid's temperature ..... K	μ	Fluid's dynamic viscosity ..... $kgm^{-1}s^{-1}$
C	Concentration of nanoparticles..... mol m^{-3}	α	Thermal diffusivity..... $m^2 s^{-1}$
N	Microbial concentration		
C_p	Specific heat of fluid ..... $Jkg^{-1}K^{-1}$	*Subscripts*	
M	Magnetic Field parameter		
$B_\circ$	Magnetic field intensity	f	Base fluid
Kp	Porosity	hnf	Hybrid nanofluid
R	Radiation parameter	s_1	TiO_2 nanoparticle
Kc	Chemical reaction parameter	s_2	Ag nanoparticle
D_B	Brownian diffusion coefficient		
D_m	Microorganisms diffusion coefficient	*Dimensionless parameter*	
		Ec	Eckert number
Greek symbols		Pr	Prandtl number
		Re	Reynold number
ρ	Fluid's density ..... kgm^{-3}	Nu	Nusselt number
σ	Electrical conductivity of fluid	Pe	Peclet number

1. Introduction

Many practical applications for stretchable surfaces such as wire design, paper and sheet production, hot rolling of components, liquid crystal solidification, food production, fibre production etc. Stretching kinematics and procedures that include both heating and cooling at the same time have a major effect concerning the standard of refined goods. The flow of a boundary layer concept was pioneered by Crane [1] through a stretched surface in two dimensions. Waini et al. [2] conducted research on the hybrid nanofluid flow on sheets that were exponentially expanded and shrunk. Viscous dissipation has been studied by Zainal et al. [3] and Rao et al. [4] in relation to the transport of nanofluids across an exponentially stretched surface.

Enhancing heat transfer is a critical challenge in the current engineering and industrial landscape. Some common fluids are not ideal for the purpose of heat transmission due to their poor thermal conductivity, therefore, their usage in heat transfer processes is limited. New fluids such as nanofluids are being developed to enhance thermal efficiency. Nanofluids have many useful uses, such as in refrigeration and air conditioning, microelectronics, computer processors etc, where they serve as coolants, lubricants, and other functions. Choi and Eastman [5] coined the term "nanofluid" to describe a liquid that exhibits highly conductive properties for heat transfer fluids, achieved through the dispersion of nanoscale-sized atoms throughout the substance. Makinde and Aziz [6] investigated the flow of nanofluids in the boundary layer across an stretched surface. However, researchers are currently looking for a more effective working fluid. To combat this issue, a novel class of nanofluids called hybrid nanofluids, has just been developed by researchers which they claim provides superior thermal conductivity. Rotational flow in a $Ag - CuO - H_2O$ hybrid nanofluid is examined by Hayat et al. [7] that is influenced by radiation and partial slip at its boundaries. Idrees et al. [8] investigates the dynamics of a three-dimensional rotating stratified Williamson hybrid nanofluid on an extended surface, incorporating the influences of single-walled carbon nanotubes (SWCNTs), multi-walled carbon nanotubes (MWCNTs), as well as suction and injection effects. Asif and Aziz [9] conducted research on a rotating stratified Williamson hybrid nanofluid flow over a stretchable sheet. Thakur and Sood [10] conducted a comparative study exploring the steady flow and heat transfer characteristics of various hybrid nanofluids when exposed to mixed convection alongside an exponentially stretching sheet. Sharma and Sood [11] and Jifeng et al. [12] investigate the behaviour of nanofluids on an inclined stretching surface within porous media, utilizing the Darcy-Forchheimer model. Other related studies to nanofluid and hybrid nanofluid with magnetic and thermal radiation effects can be explored in the existed literature ([13–18]).

Nanofluids with MHD effects are known to be able to keep in order the flow and improve transfer of heat in fluids that carry electricity. MHD thermophoretic flow's capacity for efficient heat and mass transmission has applications in air filtration, aerosol particle monitoring, nuclear reactor security, and microelectronics. Andersson [19] gave a description of MHD flow on an exponential surface taking viscoelasticity into account. Chamkha and Issa [20] used a flat plate as either a heat source or a heat sink in their study on thermophoresis in MHD flows. Triple solutions were discovered when micropolar nanofluids were subjected to MHD flow analysis by Ali et al. [21]. According to their stability analysis, only the first solution holds up during repeated use. Aly and Pop [22] compared the sheet flow of a hybrid nanofluid and regular nanofluid at their respective MHD stagnation points that is simultaneously being stretched and shrunk. Hayat et al. [23] investigated the relationship between chemical processes and convective heat transfer in a viscous nanofluid flowing over a stretched sheet. Nadeem et al. [24], conducted numerical study of the Maxwell fluid's behaviour when it encounters nanoparticles in a stretched sheet.

Viscous dissipation changes temperature profile and consequently the heat transfer efficiencies because it acts as an energy source. Viscous dissipation measures have different effects depending on whether the sheet is cold or warm. There are numerous processes that can influence the rate at which heat transfer is enhanced, such as diffusion in the Brownian regime, radiation, viscous dissipation, suction and injection. Several researchers, Rashad et al. [25] looked into how MHD and heat source affected a Cu-water nanofluid

with the aid of porous materials. It has been found by Kameswaran et al. [26] that the joint result along with viscous dissipation and magnetic fields can increase thermal production similarly decrease thermal transmission on the boundary layer. Partha et al. [27] conducted a study on the rate of heat transmission in convection flow over an exponentially stretched sheet, as well as its correlation with viscous dissipation. Further, Sajid and Hayat [28] extended this problem, who used homotopy analysis to provide an analytical solution after studying radiation's impact on the rate of flow in a sheet stretched exponentially.

Thermal radiation is an essential component in numerous manufacturing domains, encompassing electricity generation, glass production, solar energy technology and furnace construction. At high operating temperatures, the effect of radiation might become noticeable. The comprehension of thermal radiation is pivotal in the development of suitable machinery for various engineering processes that require high temperatures, stated in Seddeek [29]. Sheikholeslami and Shehzad [30] recently investigated thermal radiation of a ferrofluid subject to Lorentz forces. They found that a rise in temperature caused a rise in heat transfer's rates. Nanofluids with variable surface heat flows are analysed by Zhang et al. [31], who consider the effects of MHD or radiation. Bagh et al. [32] looked into how suction/injection affects gravity modulation mixed convection in micropolar fluid flow with an inclined sheet, magnetic field, and thermal radiation. Bakar et al. [33] conducted an examination of mixed convection within a porous medium, incorporating heat generation, suction/injection, thermal radiation, and magnetic field effects, while utilizing a hybrid $Ag - TiO_2/water$ nanofluid.

The movement of microbes in a certain direction creates bioconvection, consequently leading to an expansion of the volume of the surrounding fluid. The upward swimming of a sizable proportion of gyrotactically motile microorganisms induces convection, which leads to an increased concentration of optically duplicated apparent fluid motions for any microbe swimming in the water. Bioconvection of nanoparticles on a horizontal convective surface was conducted by Kuznetsov and Avramenkov [34]. Khan et al. [35] explained how bioconvection works in the Buongiorno nanofluid model, which consists of two elongated spinning discs. The second-grade convection flow in nanofluids was analysed by Shafiq et al. [36] based on mass and heat transmission rate and cellular motility. Kairi et al. [37] used inclined expanding plates to examine bioconvective fluid made up from motile microbe aggregation in nonlinear heat radiation, viscous dispersion, electrochemical processes, and electromagnet field. Shah et al. [38] conducted a study on stretching sheets, examining bio-convection, inclined magnetohydrodynamics, thermal linear radiations, and chemical reactions in hybrid nanofluids. Aziz et al. [39] investigated bioconvection phenomena in a Williamson nanofluid with small metallic particles suspended over a sheet. Additional research on bioconvection with motile microorganisms over a stretching sheet can be explored in existing literature ([40,41]).

The current work examines the two dimensional, incompressible boundary-layer bioconvective magnetized hybrid nanofluid flow over a sheet that has been stretched exponentially. The profiles of the governing equations are shown with behaviour of important flow parameters. Furthermore, a tabulated presentation of the drag coefficients, Nusselt numbers, Sherwood numbers and densities of motile microorganisms is included. The previous and current data are compared and evaluated subjectively. Current research is useful in several fields, including metal spinning, plastic film drawing, glass blowing, growth of crystal and filaments cooling [42,43].

To the best of the author's knowledge, no prior publications have explored this model's application employing the local non-similarity method. The primary goal of this article is to improve heat transfer efficiency within a hybrid nanofluid. Furthermore, this research holds potential significance for scholars engaged in the study of thermal systems and solar energy harvesting. This article contains the following novelties:

- Impacts of radiation, heat production, chemical reaction, permeability and viscous dissipation are considered.
- LNS technique is implemented to truncate analytically non-similar equations via the bvp4c algorithm, which is a built-in MATLAB solver.
- Silver and titanium dioxide in a water-based medium are the prototypical nanoparticles.

The present description continues its pursuit to address the following questions:

- How does the important parameters affect the flow profiles?
- What is the advantage of local non-similarity technique?
- How does hybrid nanofluid change the rates of heat and mass transfer?

2. Mathematical formulation

The incompressible steady-state hybrid nanofluid flow in two-dimensions as well as the influence of MHD and bioconvection phenomena are presented in this model and exponentially stretching sheet is used as the basis for initiation. The coordinate system chosen for this analysis entails the x-axis being aligned with the stretching surface and the y-axis being orthogonal to it (Fig. 1). The exponential stretching velocity of a sheet in the x direction ($x \geq 0$) is defined by the function $u_w(x) = U_0 e^{\frac{x}{l}}$, where U_0 is a positive constant and l is the characteristic length scale. $B(x) = B_0 e^{\frac{x}{2l}}$ is a magnetic field that can vary, where B_0 has a constant magnetic strength which is surface-normal. A variable heat source $Q(x) = Q_0 e^{\frac{x}{l}}$, chemical reaction $K_l = K_0 e^{\frac{x}{l}}$, and porosity $K = K_r e^{-\frac{x}{l}}$ impacts are taken into account as well. This model's mathematical expressions are laid out as follows [44,45]:

$$\left(\frac{\partial u}{\partial x} + \frac{\partial v}{\partial y}\right) = 0 \tag{1}$$

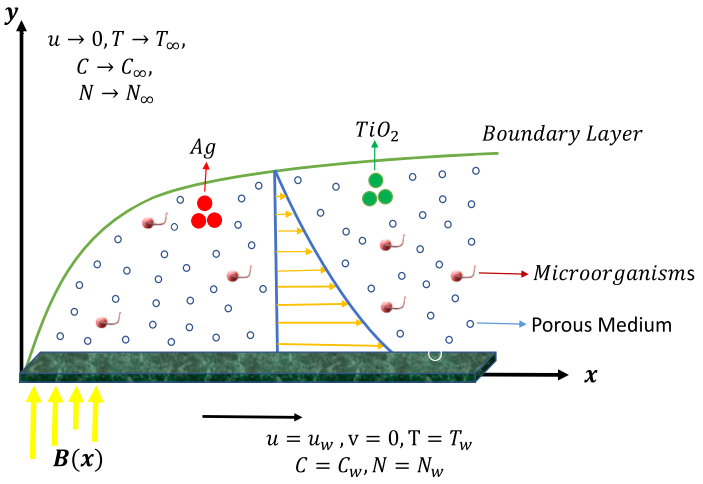

Fig. 1. Flow configuration for physical model.

$$\left(u\frac{\partial u}{\partial x}+v\frac{\partial u}{\partial y}\right)=\left(\frac{\mu_{hnf}}{\rho_{hnf}}\right)\frac{\partial^2 u}{\partial y^2}-\frac{\sigma_{hnf}}{\rho_{hnf}}B^2(x)u-\frac{\mu_{hnf}}{\rho_{hnf}}\frac{u}{K} \tag{2}$$

$$\left(u\frac{\partial T}{\partial x}+v\frac{\partial T}{\partial y}\right)=\alpha_{hnf}\frac{\partial^2 T}{\partial y^2}-\frac{1}{(\rho C_p)_{hnf}}\frac{\partial q_r}{\partial y}+\frac{Q}{(\rho C_p)_{hnf}}(T-T\infty)+\frac{\mu_{hnf}}{(\rho C_p)_{hnf}}\left(\frac{\partial u}{\partial y}\right)^2 \tag{3}$$

$$\left(u\frac{\partial C}{\partial x}+v\frac{\partial C}{\partial y}\right)=D_B\frac{\partial^2 C}{\partial y^2}-K_l(C-C_\infty) \tag{4}$$

$$\left(u\frac{\partial N}{\partial x}+v\frac{\partial N}{\partial y}\right)+\frac{bW_c}{C_w-C_\infty}\left(\frac{\partial}{\partial y}\left(N\frac{\partial C}{\partial y}\right)\right)=D_m\frac{\partial^2 N}{\partial y^2} \tag{5}$$

Within the expressions mentioned above (Eqs. (1)-(5)), the variables denoted by u and v represent the velocities along the x and y axes, respectively. And μ_{hnf}, ρ_{hnf}, σ_{hnf}, α_{hnf}, Cp_{hnf}, T, T_∞, C, C_∞, D_B, N, N_∞, and D_m represent dynamic viscosity, nanofluid density, electrical conductivity, thermal diffusivity, specific heat, temperature, freestream temperature, concentration of nanoparticle, ambient concentration of nanoparticles, Brownian diffusion coefficient, microbial concentration, ambient concentration of microorganism and microorganisms diffusion coefficient respectively. Equation (3) describes radiative heat flux: $q_r=-\frac{4\sigma^*}{3k^*}\frac{\partial T^4}{\partial y}$, here σ^* is the Stefan-Boltzman constant and k^* is the average absorption coefficient. Incorporating series of Taylor, T^4 one way to put it is $T^4=4(T_\infty^3)T-3(T_\infty^4)$.

The following conditions (Eqn. (6)) are assumed at the surface and far away from the surface:

$$\begin{aligned} at \quad y=0, \quad u=u_w=U_0e^{\frac{x}{l}}, \quad v=0, \quad T=T_w, \quad C=C_w, \quad N=N_w \\ as \quad y\to\infty, \quad u\to 0, \quad T\to T_\infty, \quad C\to C_\infty, \quad N\to N_\infty \end{aligned} \tag{6}$$

Non-similar transformation is as follows [46]

$$\begin{aligned} \xi=e^{\frac{x}{l}}, \quad \eta=ye^{\frac{x}{2l}}\sqrt{\frac{U_0}{2\nu l}}, \quad u=U_0e^{\frac{x}{l}}\frac{\partial f}{\partial \eta}, \quad v=\sqrt{\frac{\nu U_0}{2l}}e^{\frac{x}{2l}}\left[f+\eta\frac{\partial f}{\partial y}+2\xi\frac{\partial f}{\partial \xi}\right] \\ \theta(\xi,\eta)=\frac{T-T_\infty}{T_w-T_\infty}, \quad \phi(\xi,\eta)=\frac{C-C_\infty}{C_w-C_\infty}, \quad \chi(\xi,\eta)=\frac{N-N_\infty}{N_w-N_\infty} \end{aligned} \tag{7}$$

$$\frac{\mu_{hnf}}{\mu_f}=\frac{1}{a_1}, \frac{\rho_{hnf}}{\rho_f}=a_2, \frac{\sigma_{hnf}}{\sigma_f}=a_3, \frac{(\rho Cp)_{hnf}}{(\rho Cp)_f}=a_4, and \frac{k_{hnf}}{k_f}=a_5 \tag{8}$$

Equations (1)–(6) can be converted into the following information in light of the non-similarity variables (Eq. (7)) and efficient thermophysical model (Table 1):

$$\frac{\partial^3 f}{\partial \eta^3}+a_1a_2f\frac{\partial^2 f}{\partial \eta^2}-\left((a_1a_3M+K_p)+2a_1a_2\frac{\partial f}{\partial \eta}\right)\frac{\partial f}{\partial \eta}-2a_1a_2\xi\left(\frac{\partial f}{\partial \eta}\frac{\partial^2 f}{\partial \xi\partial \eta}-\frac{\partial f}{\partial \xi}\frac{\partial^2 f}{\partial \eta^2}\right)=0 \tag{9}$$

Table 1
Visualisation of thermophysical characteristics is provided by [47].

Property	Nanomaterials
Dynamic Viscosity	$\frac{\mu_{hnf}}{\mu_f} = \left((1-\phi_1)^{2.5}(1-\phi_2)^{2.5}\right)^{-1}$
Density	$\frac{\rho_{hnf}}{\rho_f} = \left((1-\phi_2)\left[1-\phi_1+\phi_1\left(\frac{\rho_{s1}}{\rho_f}\right)\right]\right)+\left(\phi_2\left(\frac{\rho_{s2}}{\rho_f}\right)\right)$
Electrical conductivity	$\frac{\sigma_{hnf}}{\sigma_f} = 1+\frac{3\left(\frac{\phi_1\sigma_1+\phi_2\sigma_2}{\sigma_f}-(\phi_1+\phi_2)\right)}{2+\left(\frac{\phi_1\sigma_1+\phi_2\sigma_2}{(\phi_1+\phi_2)\sigma_f}\right)-\left(\frac{\phi_1\sigma_1+\phi_2\sigma_2}{\sigma_f}-(\phi_1+\phi_2)\right)}$
Specific Heat	$\frac{(\rho Cp)_{hnf}}{(\rho Cp)_f} = \left((1-\phi_2)\left[1-\phi_1+\phi_1\left(\frac{(\rho Cp)_{s1}}{(\rho Cp)_f}\right)\right]\right)+\left(\phi_2\left(\frac{(\rho Cp)_{s2}}{(\rho Cp)_f}\right)\right)$
Thermal conductivity	$\frac{k_{hnf}}{k_f} = \frac{k_{s2}+2k_{nf}-2\phi_2(k_{nf}-k_{s2})}{k_{s2}+2k_{nf}+2\phi_2(k_{nf}-k_{s2})}$ and $\frac{k_{nf}}{k_f} = \frac{k_{s1}+2k_f-2\phi_1(k_f-k_{s1})}{k_{s1}+2k_f+2\phi_1(k_f-k_{s1})}$

$$a_1\left(a_5+\frac{4}{3}R\right)\frac{\partial^2\theta}{\partial\eta^2}+a_1a_4Prf\frac{\partial\theta}{\partial\eta}+EcPr\xi^2\left(\frac{\partial^2 f}{\partial\eta^2}\right)^2+a_1\beta Pr\theta -2a_1a_4\xi Pr\left(\frac{\partial f}{\partial\eta}\frac{\partial\theta}{\partial\xi}-\frac{\partial f}{\partial\xi}\frac{\partial\theta}{\partial\eta}\right)=0 \tag{10}$$

$$\frac{\partial^2\phi}{\partial\eta^2}+Lef\frac{\partial\phi}{\partial\eta}-KcLe\phi-2\xi Le\left(\frac{\partial f}{\partial\eta}\frac{\partial\phi}{\partial\xi}-\frac{\partial f}{\partial\xi}\frac{\partial\phi}{\partial\eta}\right)=0 \tag{11}$$

$$\frac{\partial^2\chi}{\partial\eta^2}+Lbf\frac{\partial\chi}{\partial\eta}-Pe\left(\frac{\partial\chi}{\partial\eta}\frac{\partial\phi}{\partial\eta}+(\chi+\Omega)\frac{\partial^2\phi}{\partial\eta^2}\right)-2\xi Lb\left(\frac{\partial f}{\partial\eta}\frac{\partial\chi}{\partial\xi}-\frac{\partial f}{\partial\xi}\frac{\partial\chi}{\partial\eta}\right)=0 \tag{12}$$

Boundary conditions:

$$\frac{\partial f}{\partial\eta}(\xi,0)=1,\quad f(\xi,0)+2\xi\frac{\partial f}{\partial\xi}(\xi,0)=0,\quad \theta(\xi,0)=1,\quad \phi(\xi,0)=1$$
$$\chi(\xi,0)=1,\quad \frac{\partial f}{\partial\eta}(\xi,\infty)=0,\quad \theta(\xi,\infty)=0,\quad \phi(\xi,\infty)=0,\quad \chi(\xi,\infty)=0 \tag{13}$$

In the aforementioned Eqs. (9)-(13), M, Kp, R, Kc demonstrates magnetic field, porosity parameter, radiation and chemical reaction parameters, whereas Pr, Ec, Le, Lb, Pe, β and Ω are Prandtl number, Ecker number, Lewis number, Lewis number of bioconvection, Peclet number of bioconvection, heat source with no dimensions and the concentration of microbes difference parameter respectively (Eqn. (14)), which are mentioned below.

$$M=\frac{2lB_0^2\sigma_f}{U_0\rho_f},Kp=\frac{2l\nu_f}{K_rU_0},R=\frac{4\sigma^*T_\infty^3}{k^*k_f},Pr=\frac{\mu_f(Cp)_f}{k_f},Ec=\frac{U_0^2}{(Cp)_f(T_w-T_\infty)}$$
$$\beta=\frac{2lQ_0}{U_0(\rho Cp)_f},Le=\frac{\nu_f}{D_B},Kc=\frac{2lK_0}{U_0},Lb=\frac{\nu_f}{D_m},Pe=\frac{bW_c}{D_m},\Omega=\frac{N_\infty}{(N_w-N_\infty)} \tag{14}$$

the symbols μ_f, ρ_f, σ_f, k_f, and $(\rho Cp)_f$ denote the viscosity, density, electrical conductivity, thermal conductivity and heat capacity of the base fluids, respectively.

3. Local non-similarity method

The utilisation of a local non-similarity technique, first introduced by Sparrow et al. [48] and later advanced by Yu and Sparrow [49], was proposed as a means to obtain solutions for the non-similar boundary layers.

3.1. First truncation level

In order to achieve first level truncation, terms that are accompanied by $\xi\frac{\partial}{\partial\xi}$ are regarded as negligibly small. Thereby, the governing system transformed into Eqs. (15)-(19):

$$f'''+a_1a_2ff''-\left(\left(a_1a_3M+Kp\right)+2a_1a_2f'\right)f'=0 \tag{15}$$
$$a_1\left(a_5+\frac{4}{3}R\right)\theta''+a_1a_4Prf\theta'+EcPr\xi^2\left(f''\right)^2+a_1\beta Pr\theta=0 \tag{16}$$
$$\phi''+Lef\phi'-KcLe\phi=0 \tag{17}$$
$$\chi''+Lbf\chi'-Pe\left(\chi'\phi'+(\chi+\Omega)\phi''\right)=0 \tag{18}$$

The boundary conditions for 1^{st} truncation are:

$$f'(\xi,0)=1,\quad f(\xi,0)=0,\quad \theta(\xi,0)=1,\quad \phi(\xi,0)=1,\quad \chi(\xi,0)=1$$
$$f'(\xi,\infty)=0,\quad \theta(\xi,\infty)=0,\quad \phi(\xi,\infty)=0,\quad \chi(\xi,\infty)=0 \tag{19}$$

3.2. Second truncation level

We took into account the following for the second level of truncation:

$$\frac{\partial f}{\partial \xi} = A, \quad \frac{\partial \theta}{\partial \xi} = B, \quad \frac{\partial \phi}{\partial \xi} = G, \quad \frac{\partial \chi}{\partial \xi} = H \tag{20}$$

In light of the above, the system of 2^{nd} truncation level is contained the Eqns. (21)-(25):

$$A''' + a_1 a_2 \left(f A'' + 3Af'' + 2f'A' - 2\xi \left(A'^2 - AA'' \right) \right) - \left(a_1 a_3 M + Kp \right) A' = 0 \tag{21}$$

$$\left(\frac{1}{a_1 \left(a_5 + \frac{4}{3} R \right)} \right) B'' + a_1 a_4 Pr \left(f B' + A\theta' - 2 \left(f'B - A\theta' + \xi \left(BA' - AB' \right) \right) \right) + a_1 \beta Pr B + 2Ec Pr \left(\xi^2 f'' A'' + \xi \left(f'' \right)^2 \right) = 0 \tag{22}$$

$$G'' + Le(fG' - 2f'G) + 3Le\phi' A - KcLeG - 2Le\xi(GA' - AG') = 0 \tag{23}$$

$$H'' + Lb(fH' - 2f'H) + 3Lb\chi' A - Pe(\chi' G' + (\chi + \Omega)G'' + (\phi' H' + \phi'' H)) - 2Lb\xi(HA' - AH') = 0 \tag{24}$$

The boundary conditions for 2^{nd} truncation are:

$$\begin{gathered} A'(\xi,0) = 0, \quad A(\xi,0) = 0, \quad B(\xi,0) = 0, \quad G(\xi,0) = 0, \quad H(\xi,0) = 0 \\ A'(\xi,\infty) = 0, \quad B(\xi,\infty) = 0, \quad G(\xi,\infty) = 0, \quad H(\xi,\infty) = 0 \end{gathered} \tag{25}$$

4. Significant physical quantities

The study by Waini and Ishak [2] and Pal and Mondal [45] documented the coefficient of skin friction, Nusselt number, Sherwood number and density number for movable microorganisms.

$$\begin{gathered} Cf_x = \frac{\tau_w}{\rho_f (u_w)^2}, \quad Nu_x = \frac{l q_w}{k_f (T_w - T_\infty)} \\ Sh_x = \frac{l q_m}{D_B (C_w - C_\infty)}, \quad Nn_x = \frac{l q_n}{D_m (N_w - N_\infty)} \end{gathered} \tag{26}$$

where

$$\tau_w = \rho_{hnf} \frac{\partial u}{\partial y}, \quad q_w = -k_{hnf} \frac{\partial T}{\partial y} + q_r, \quad q_m = -D_B \frac{\partial C}{\partial y}, \quad q_n = -D_m \frac{\partial N}{\partial y} \tag{27}$$

Our final result is the dimensionless form seen below (Eqn. (28)).

$$\begin{gathered} Re_x^{\frac{1}{2}} Cf_x = \frac{f''(\xi,0)}{a_1 \sqrt{2\xi}}, \quad Re_x^{-\frac{1}{2}} Nu_x = -\sqrt{\frac{\xi}{2}} \left(a_5 + \frac{4}{3} R \right) \theta'(\xi,0) \\ Re_x^{-\frac{1}{2}} Sh_x = -\sqrt{\frac{\xi}{2}} \phi'(\xi,0), \quad Re_x^{-\frac{1}{2}} Nn_x = -\sqrt{\frac{\xi}{2}} \chi'(\xi,0) \end{gathered} \tag{28}$$

where $Re_x = \frac{l U_0}{\nu_f}$ is the local Reynold's number.

5. Method of solution

It appears challenging to find out the most appropriate result under consideration since the partial differential system Eqs. (9)-(12) subjected to Eq. (13) exhibits nonlinearity. To get to a quick and effective solution under consideration, therefore combined numerical algorithm bvp4c with analytic LNS technique till the second truncation (Eqs. (15)–(25)). Using the following presumptions, we complete the process:

$$\begin{gathered} f = f(1), \quad f' = f(2), \quad f'' = f(3), \quad \theta = f(4), \quad \theta' = f(5), \quad \phi = f(6), \\ \phi' = f(7), \quad \chi = f(8), \quad \chi' = f(9), \quad A = f(10), \quad A' = f(11), \quad A'' = f(12), \\ B = f(13), \quad B' = f(14), \quad G = f(15), \quad G' = f(16), \quad H = f(17), H' = f(18) \end{gathered} \tag{29}$$

The efficiency of this method has become increasingly popular while remaining on par with other techniques. An approximation of the numerical simulation error is provided by the residual error module in the MATLAB package known as bvp4c. This study's tabular data and graphical simulations both pass the bvp4c tolerance requirements (10^{-3}).

Table 2
Thermophysical properties [43].

Property	H_2O	TiO_2	Ag
ρ	997.1	4250	10,500
C_p	4179	686.2	235
k	0.613	8.9538	429
σ	5×10^{-2}	2.38×10^{6}	3.5×10^{6}

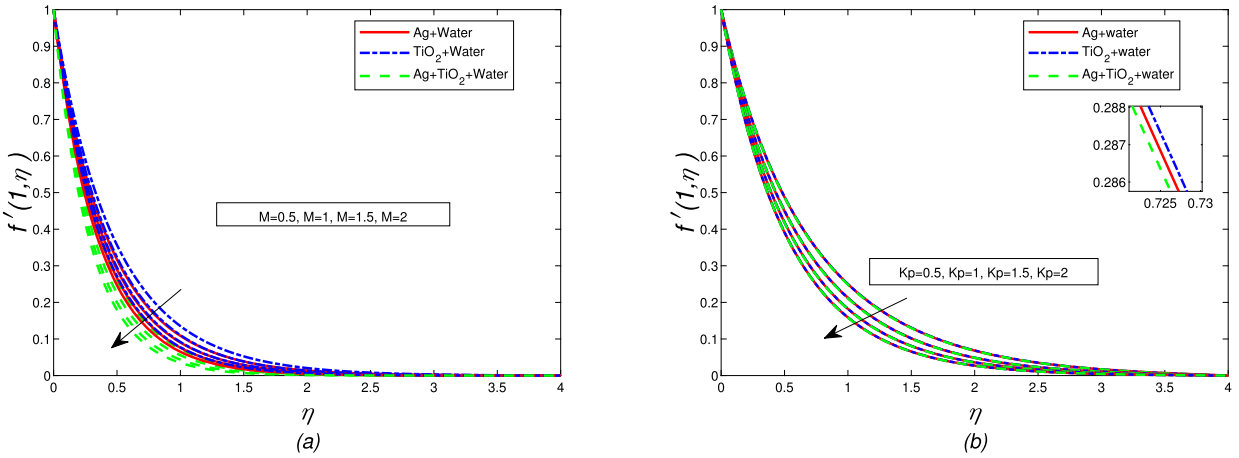

Fig. 2. (a) Implications of M, **(b)** Kp, on $f'(1,\eta)$ respectively, when $\beta=0.1$, $Pr=6.2$, $Ec=0.3$, $Le=2$, $R=Kc=0.1$, $=Pe=\Omega=0.5$, $Lb=1.20$, $\xi=1$.

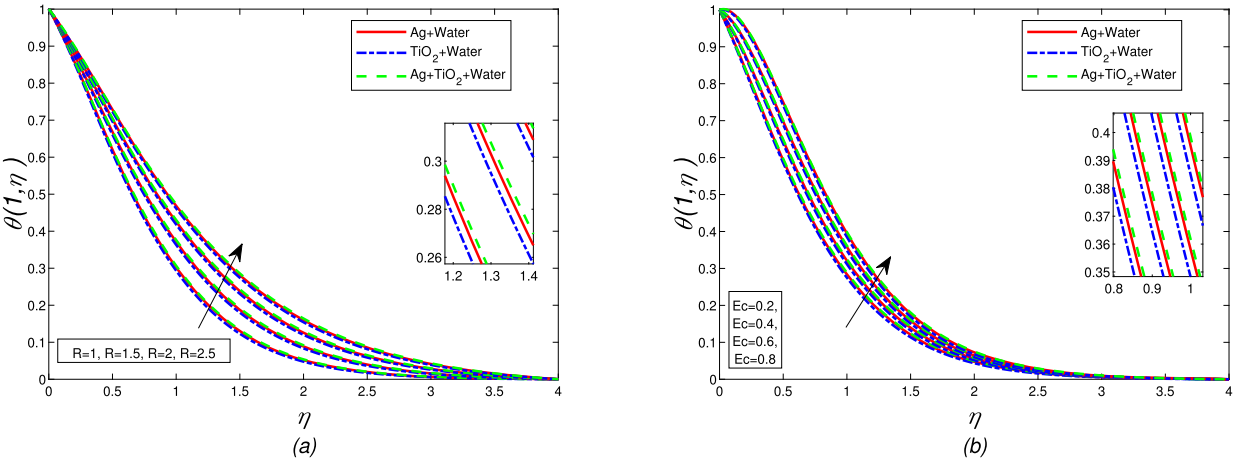

Fig. 3. (a) Implications of R, **(b)** Ec, on $\theta(1,\eta)$ respectively, when $\beta=Kc=Kp=M=0.1$, $=Pe=\Omega=0.5$, $Pr=6.2$, $Le=2$, $Lb=1.2$, $\xi=1$.

6. Discussion and results

The effect of relevant factors affecting velocity, temperature, nanoparticle concentration and microbial concentration distributions are demonstrated in Figs. 2–7. Water and nanoparticles of (TiO_2 and Ag) are shown in Table 2 along with their respective thermophysical data.

6.2 is fixed for Prandtl number and $0.5\leq M, Kp, Kc\leq 2$, $0.1\leq\beta, Pe, \Omega\leq 0.4$, $1\leq Le, R\leq 2.5$, $0.2\leq Lb, Ec\leq 0.8$ show the range of parameters in our computations for convergent solutions.

As seen in Fig. 2(a), the velocity tends to drop as the magnetic parameter (M) rises. As magnetic field parameter (M) increases the Lorentz force is generated. The fluid's motion is resisted by the Lorentz force and hence it slows the velocity. Fig. 2(b) demonstrates how the porosity (Kp) has a negative influence in the velocity distribution. The phenomenon of porosity causes resistance to fluid flow and slows it down. Whenever Kp grows, the fluid slows down because the amplitude of the Darcian body force decreases. Fig. 3(a) displays the impact of radiation (R) on $\theta(1,\eta)$. When R is increased, temperature of the fluid rises because more heat is being radiated from surface level. As can be seen from Fig. 3(b) that $\theta(1,\eta)$ is positively affected by Eckert number (Ec). This phenomenon can be attributed to an increase in drag forces between the fluid materials. A rise in temperature can be explained

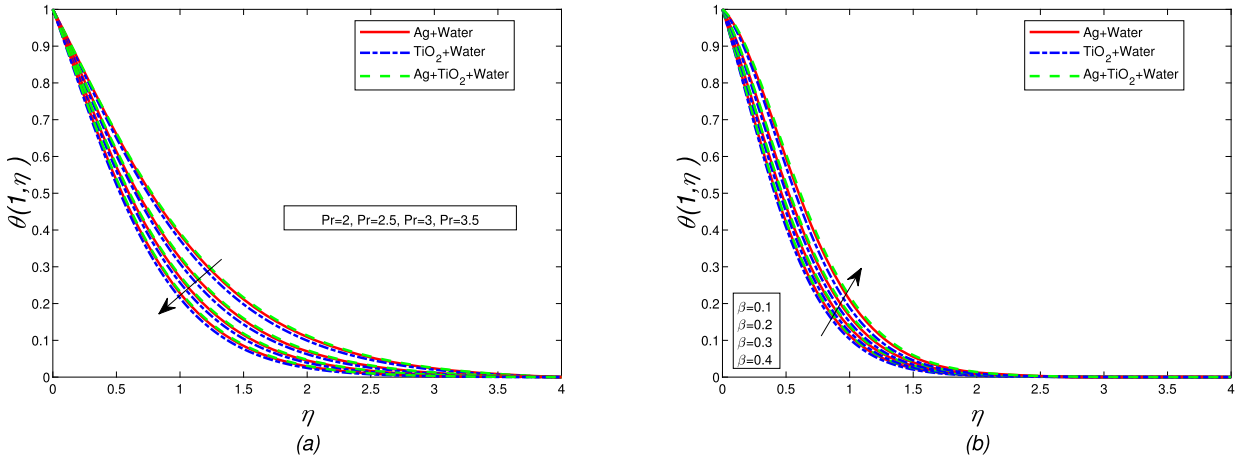

Fig. 4. (a) Implications of Pr, **(b)** β, on $\theta(1,\eta)$ respectively, when $R = Kc = Kp = M = 0.1$, $= Pe = \Omega = 0.5$, $Ec = 0.3$, $Le = 2$, $Lb = 1.2$, $\xi = 1$.

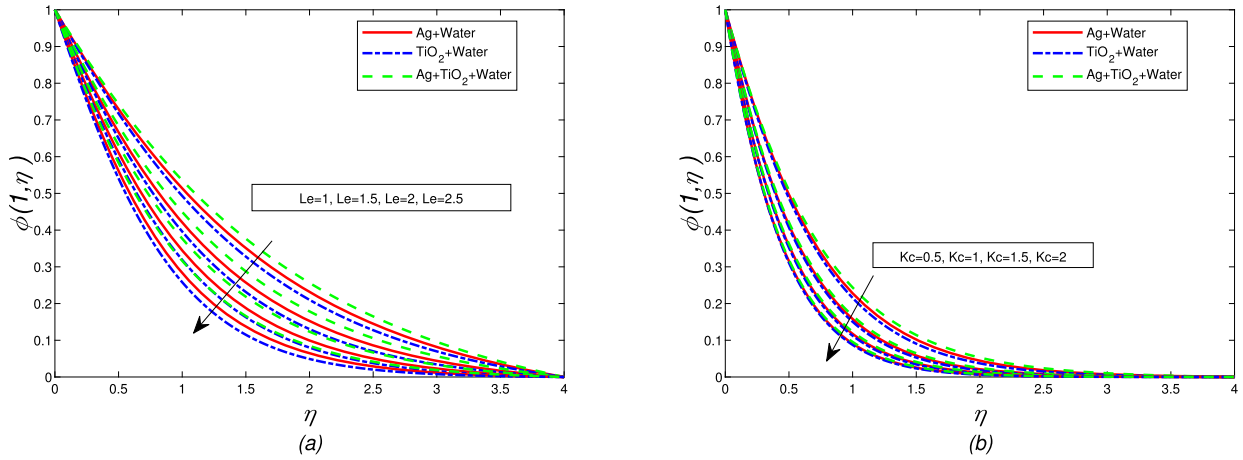

Fig. 5. (a) Implications of Le, **(b)** Kc, on $\phi(1,\eta)$ respectively, when $R = Kp = M = \beta = 0.1$, $= Pe = \Omega = 0.5$, $Pr = 6.2$, $Ec = 0.3$, $Lb = 1.2$, $\xi = 1$.

because there are collisions between fluid particles, so the temperature rises and hence generate frictional energy. Fig. 4 (a) indicates that the consequences of increasing Pr lead to decline in the temperature profile. The ratio of momentum and thermal diffusivity is indicated by the Prandtl number. So, it is sure that the enhancement in Pr decreases the thermal boundary layer thickness. Heat source parameter β creates internal heat, which raises the temperature profile in Fig. 4(b). The thermal source increases the thickness of the thermal boundary layer by adding heat to the layer. The concentration profile seen in Fig. 5(a) decreases as the Lewis number (Le) increases because the mass diffusivity decreases. Rising rates of chemical reaction parameter (Kc) speeds up consumption of the nanoparticles, resulting in a decrease in $\phi(1,\eta)$, as seen in Fig. 5(b). Fig. 6(a) shows that increase in bioconvection Lewis number (Lb), so fluid motile density decreases, and the microbes diffuse more slowly. With increasing Peclet number results in the decrease in $\chi(1,\eta)$ as seen in Fig. 6(b). Increase in Pe physically speeds up microbial motion, decreasing motile density close to the surface [45]. The variations in $\chi(1,\eta)$ as a function of the Ω parameter describing the differences in microbial concentration are depicted in Fig. 7. Higher values of $\Omega(1,\eta)$ imply that between the gyrotactic microorganisms and the base fluid, greater density difference making unstable fluid surface and inducing the microbes to move back to the bottom of fluid, causing a reduction in $\chi(1,\eta)$. The comparison of numerical result vs the results of Magyari and Keller [50] as well as El- Aziz [51] for validation are represented in Table 3 below. In Tables 4–7, we examine the effect of well-known factors, coefficient of skin friction, Nusselt, Shwerwood and motile density numbers.

- Variations in M and Kp from Table 4 lead to a greater drag coefficient.
- In Table 5 bellow, as Le and Kc rise, so does the corresponding local Sherwood number.
- As seen in Table 6, whenever values of Lb, Pe, and Ω are increased, the local motile density number rises.
- As R increases the surface heat flow, heat transfer rises, but it lowers overall when the values of Ec, β rise as seen in Table 7. These factors create internal heat which lowers the surface-to-fluid temperature difference and also thermal conduction's rate.

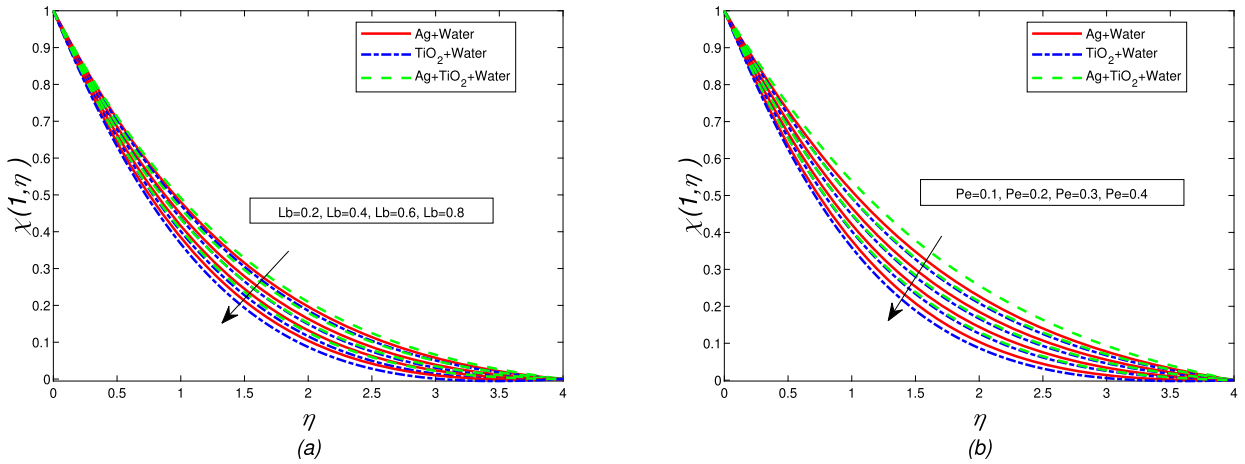

Fig. 6. (a) Implications of Lb, **(b)** Pe, on $\chi(1,\eta)$ when $Ec = 0.03$, $M = R = Kc = Pe = 0.5$, $Pr = 6.2$, $Kp = 1$, $\Omega = 6$, $\beta = Le = 0.1$ $Lb = 1.2$.

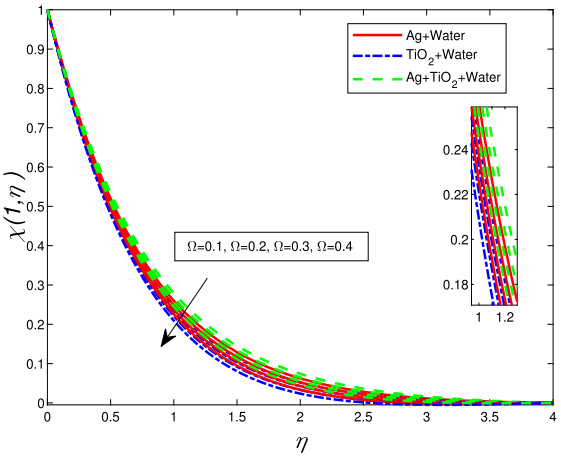

Fig. 7. Implication of Ω on $\chi(1,\eta)$, when $M = 0.2$, $\beta = R = Le = 0.1$, $Pe = 2.5$, $= Kc = 0.5$, $Ec = 0.03$ $Pr = 6.2$, $Lb = 1.2$, $\xi = 1$.

Table 3
A comparative analysis of $-\theta'(0)$ for discrete values of Pr if $\phi_1 = \phi_2 = M = Kp = R = Ec = \beta = Le = Kc = Lb = Pe = \Omega = \xi = 0$.

Pr	Magyari [50]	Aziz [51]	Present Study
1	0.549643	0.549644	0.549851
3	1.122188	1.122087	1.122076
5	1.521243	1.521239	1.521234
10	2.257429	2.257424	2.257427

Table 4
Variation in $Re_x^{\frac{1}{2}} Cf_x$ for $Le = 2$, $Kc = \Omega = Pe = 0.5$, $Lb = 1.2$, $Pr = 6.2$, $R = 1$, $Ec = 0.3$, $\beta = 0.1$.

M	Kp	Ag	TiO_2	$Ag + TiO_2$
0.5		-2.0570003051	-1.8149090273	-2.4725459874
1		-2.2000138668	-1.9752188267	-2.6746559602
1.5		-2.3340639513	-2.1232738040	-2.8621604687
2		-2.4606896286	-2.2615516407	-3.0379062811
	0.5	-0.2594998775	-0.2308065526	-0.3194456082
	1	-0.2694455692	-0.2419139132	-0.3275771175
	1.5	-0.2790280585	-0.2525255459	-0.3355056986
	2	-0.2882855423	-0.2627034277	-0.3432469247

Table 5
Variation in $Re_x^{-\frac{1}{2}} Sh_x$ for $Pr = 6.2$, $R = 1$, $Ec = 0.3$, $\Omega = Pe = 0.5, \beta = 0.1$ and $Lb = 1.2$.

Le	Kc	Ag	TiO_2	$Ag + TiO_2$
1		0.1573895535	0.1577012649	0.1567759043
1.5		0.1935215000	0.1938890971	0.1927922096
2		0.2240569450	0.2244653879	0.2232423046
2.5		0.2510016825	0.2514420663	0.2501198212
	0.5	0.1783698119	0.1801053489	0.1748816497
	1	0.2263414302	0.2275040074	0.2240078768
	1.5	0.2653542817	0.2662436537	0.2635649802
	2	0.2991317157	0.2998580900	0.2976666472

Table 6
Variation in $Re_x^{-\frac{1}{2}} Nn_x$ for $Pr = 6.2$, $R = 1$, $Ec = 0.03$, $\beta = Le = 0.1$.

Lb	Pe	Ω	Ag	TiO_2	$Ag + TiO_2$
0.2			0.0629679846	0.0640486231	0.0616335041
0.4			0.0672190986	0.0686803923	0.0654028919
0.6			0.0715213243	0.0733480827	0.0692328599
0.8			0.0758404724	0.0780079216	0.0730997767
	0.1		0.1309698938	0.1370201889	0.1233198989
	0.2		0.1485366564	0.1548048499	0.1405681181
	0.3		0.1663537093	0.1728326783	0.1580766049
	0.4		0.1844124092	0.1910954283	0.1758363337
		0.1	0.6141725173	0.6162055949	0.6121393653
		0.2	0.6158812901	0.6179175007	0.6138450017
		0.3	0.6175900630	0.6196294066	0.6155506382
		0.4	0.6192988358	0.6213413124	0.6172562747

Table 7
Variation in $Re_x^{-\frac{1}{2}} Nu_x$ for $Pr = 6.2$, $Ec = 0.3$, $Le = 2$, $\Omega = Pe = 0.5, \beta = 0.001$, $Kc = 0.1$, $Lb = 1.2$.

R	Ec	Pr	β	Ag	TiO_2	$Ag + TiO_2$
1				0.9709077017	1.0125761063	0.9520046909
1.5				1.1102109936	1.1540615475	1.0888884435
2				1.2332569176	1.2784917800	1.2101575116
2.5				1.3478378968	1.3938754394	1.3235025948
	0.2			0.4425545310	0.5931047011	0.3922780334
	0.4			0.4363324423	0.5856308241	0.3861977361
	0.6			0.4301103535	0.5781569470	0.3801174390
	0.8			0.4238882648	0.5706830701	0.3740371417
		2		0.5363417783	0.5554962217	0.5296100314
		2.5		0.6138106388	0.6356236041	0.6063281186
		3		0.6848838329	0.7088083985	0.6768662766
		3.5		0.7502497352	0.7759648427	0.7418153581
			0.1	0.1225844281	0.1615351074	0.1084227113
			0.2	0.0907766245	0.1255157079	0.0729334120
			0.3	0.0512410989	0.0800801457	0.0272742907
			0.4	-0.0013496728	0.0172537937	-0.0367422389

7. Final observations

Bioconvective MHD hybrid nanofluid ($Ag + TiO_2$ in Water) with radiation, heat production, chemical reaction, permeability and viscous dissipation is investigated in this work as it flows across an exponentially extending surface. By contrast, the non-dimensionalisation process that makes the use of non-similarity transformation is a little more general, accurate and physical. After performing similarity transformations, non-similar phrases become apparent, and this is our main area of interest. The LNS technique is utilized, which includes truncating terms at various levels, potentially affecting the precision of the solution. The results are visually represented to show how the ranges for the most important aspects of the flow pattern affect the patterns of velocity, temperature, nanoparticle concentration and density of microorganisms. The required solutions of transformed system are obtained with the aid of a MATLAB programme called bvp4c. Researchers in the fields of industry and engineering may find this study interesting as they explore the various possible applications of hybrid nanofluids, such as metal spinning, plastic film drawing, glass blowing, crystal growth, filament cooling and many more. In the future, this research can be further expanded to encompass various

geometrical configurations, such as the Riga plate, inclined sheet, triangular enclosure and others. Additionally, a fluid comprising more than two nanoparticles can be employed as a functional fluid. The most important findings from the research are:

- As M and Kp parameters are increased, there is a corresponding decrease in velocity.
- Increasing R, Ec, and β levels lead to rising temperatures.
- When Pr is increased, then graph of temperature is shown to decrease.
- When both Le and Kc parameters are increased, then concentration of nanoparticles decreases.
- When Lb, Pe, and Ω these parameters grow, the microbial density decreases.
- Larger estimates in M and Kp lead as for larger drag coefficient.
- It is true that when parameters Pr and R both increases so the nusselt number increases, while a converse relationship can be observed for β and Ec.
- An increase in both Le and Kc leads to a rise in the Sherwood number.
- Elevated values of the parameters Lb, Pe and Ω indicate a corresponding rise in the density.

CRediT authorship contribution statement

Jifeng Cui: Formal analysis, Conceptualization. **Haseena:** Writing – original draft, Methodology, Formal analysis. **Umer Farooq:** Validation, Supervision, Conceptualization. **Ahmed Jan:** Writing – review & editing, Validation, Formal analysis. **Muzamil Hussain:** Writing – review & editing, Formal analysis, Conceptualization.

Declaration of competing interest

The authors declare that they have no known competing financial interests or personal relationships that could have appeared to influence the work reported in this paper.

Data availability

Data will be made available on request.

Acknowledgement

This work was supported by the National Natural Science Foundation of China (Approval Nos. 12062018, 12172333), Program for Young Talents of Science and Technology in Universities of Inner Mongolia Autonomous Region (Approval No. NJYT22075) and the Basic Science Research Fund in the Universities Directly under the Inner Mongolia Autonomous Region (JY20220063JY20220331ZTY2023014).

References

[1] L.J. Crane, Flow past a stretching plate, Z. Angew. Math. Phys. 21 (1970) 645–647, https://doi.org/10.1007/BF01587695.
[2] I. Waini, A. Ishak, I. Pop, Hybrid nanofluid flow induced by an exponentially shrinking sheet, Chin. J. Phys. 68 (2020) 468–482, https://doi.org/10.1016/j.cjph.2019.12.015.
[3] N.A. Zainal, R. Nazar, K. Naganthran, I. Pop, Viscous dissipation and MHD hybrid nanofluid flow towards an exponentially stretching/shrinking surface, Neural Comput. Appl. 33 (2021) 11285–11295, https://doi.org/10.1007/s00521-020-05645-5.
[4] A.S. Rao, K.D. Ramaiah, G. Kotha, M.V.S. Rao, A.J. Chamkha, A spectral relaxation approach for boundary layer flow of nanofluid past an exponentially stretching surface with variable suction in the presence of heat source/sink with viscous dissipation, Arab. J. Sci. Eng. 46 (2021) 7509–7520, https://doi.org/10.1007/s13369-021-05422-z.
[5] S. Choi, J. Eastman, Enhancing thermal conductivity of fluids with nanoparticles [Online]. Available https://www.osti.gov/biblio/196525. (Accessed 14 November 2022), 1995.
[6] O.D. Makinde, A. Aziz, Boundary layer flow of a nanofluid past a stretching sheet with convective boundary condition, Int. J. Therm. Sci. 50 (2011) 1326–1332.
[7] T. Hayat, S. Nadeem, A.U. Khan, Rotating flow of Ag–CuO/H2O hybrid nanofluid with radiation and partial slip boundary effects, Euro. Phys. J. E 41 (2018) 75.
[8] M. Idrees, S.A.A. Shah, B. Ahmad, B. Ali, I. Mahmood, New insights into the heat transfer dynamics of a hybrid (SWCNT-MWCNT) nanofluid: a case of 3D rotational flow, Int. Commun. Heat Mass Transf. 138 (2022) 106311.
[9] S.A.A. Shah, A.U. Awan, Significance of magnetized Darcy-Forchheimer stratified rotating Williamson hybrid nanofluid flow: a case of 3D sheet, Int. Commun. Heat Mass Transf. 136 (2022) 106214.
[10] A. Thakur, S. Sood, Comparative investigation of the mixed convective stagnated flow of $TiO_2 - CuO/water - EG$ $TiO_2 - CuO/water - EG$ hybrid nanofluids past an exponentially stretching sheet, Z. Angew. Math. Mech. (ZAMM-Journal of Applied Mathematics and Mechanics) 102 (12) (2022) e202100419.
[11] D. Sharma, S. Sood, Effect of inclined magnetic field on flow of Williamson nanofluid over an exponentially stretching surface in Darcy-Forchheimer model, Z. Angew. Math. Mech. (ZAMM-Journal of Applied Mathematics and Mechanics) 102 (6) (2022) e202100425.
[12] J. Cui, A. Jan, U. Farooq, M. Hussain, W.A. Khan, Thermal analysis of radiative Darcy–Forchheimer nanofluid flow across an inclined stretching surface, Nanomaterials 12 (23) (2022) 4291.
[13] G. Mandal, D. Pal, Dual solutions of radiative Ag-MoS2/water hybrid nanofluid flow with variable viscosity and variable thermal conductivity along an exponentially shrinking permeable Riga surface: stability and entropy generation analysis, Int. J. Model. Simul. (2023) 1–26.
[14] D. Pal, G. Mandal, Stability analysis and implication of Darcy magnetic-radiative hybrid reactive nanofluid heat transfer over a shrinkable surface with Ohmic heating, J. Therm. Anal. Calorim. 148 (5) (2023) 2087–2104.
[15] G. Mandal, Entropy analysis on magneto-convective and chemically reactive nanofluids flow over a stretching cylinder in the presence of variable thermal conductivity and variable diffusivity, J. Nanofluids 12 (3) (2023) 819–831.

[16] G. Mandal, D. Pal, Mixed convective-quadratic radiative MoS 2–SiO 2/H 2 O hybrid nanofluid flow over an exponentially shrinking permeable Riga surface with slip velocity and convective boundary conditions: entropy and stability analysis, Numer. Heat Transf., Part A, Appl. (2023) 1–26.
[17] D. Pal, G. Mandal, K. Vajravelu, W. Al-Kouz, MHD thermo-radiative heat transfer characteristics of carbon nanotubes based nanofluid over a convective expanding sheet in a porous medium with variable thermal conductivity, Int. J. Model. Simul. (2023) 1–12.
[18] G. Mandal, D. Pal, Entropy analysis of magneto-radiative SWCNT-MWCNT/H2O hybrid nanofluid flow with slip boundary conditions, Int. J. Ambient Energy 44 (1) (2023) 1017–1030.
[19] H.I. Andersson, MHD flow of a viscoelastic fluid past a stretching surface, Acta Mech. 95 (1992) 227–230.
[20] A.J. Chamkha, C. Issa, Effects of heat generation/absorption and thermophoresis on hydromagnetic flow with heat and mass transfer over a flat surface, Int. J. Numer. Methods Heat Fluid Flow 10 (4) (2000) 432–448, https://doi.org/10.1108/09615530010327404/FULL/XML.
[21] L. Ali Lund, D.L. Ching, Z. Omar, I. Khan, K.S. Nisar, Triple local similarity solutions of Darcy-Forchheimer Magnetohydrodynamic (MHD) flow of micropolar nanofluid over an exponential shrinking surface: stability analysis, Coatings 9 (8) (2019) 527.
[22] E.H. Aly, I. Pop, MHD flow and heat transfer near stagnation point over a stretching/shrinking surface with partial slip and viscous dissipation: hybrid nanofluid versus nanofluid, Powder Technol. 367 (2020) 192–205, https://doi.org/10.1016/j.powtec.2020.03.030.
[23] T. Hayat, M.B. Ashraf, S.A. Shehzad, A. Alsaedi, Mixed convection flow of Casson nanofluid over a stretching sheet with convectively heated chemical reaction and heat source/sink, J. Appl. Fluid Mech. 8 (4) (2015) 803–813, https://doi.org/10.18869/acadpub.jafm.67.223.22995.
[24] S. Nadeem, R.U. Haq, Z.H. Khan, Numerical study of MHD boundary layer flow of a Maxwell fluid past a stretching sheet in the presence of nanoparticles, J. Taiwan Inst. Chem. Eng. 45 (1) (2014) 121–126, https://doi.org/10.1016/j.jtice.2013.04.006.
[25] A.M. Rashad, M.M. Rashidi, G. Lorenzini, S.E. Ahmed, A.M. Aly, Magnetic field and internal heat generation effects on the free convection in a rectangular cavity filled with a porous medium saturated with Cu–water nanofluid, Int. J. Heat Mass Transf. 104 (2017) 878–889, https://doi.org/10.1016/j.ijheatmasstransfer.2016.08.025.
[26] P.K. Kameswaran, M. Narayana, P. Sibanda, P.V.S.N. Murthy, Hydromagnetic nanofluid flow due to a stretching or shrinking sheet with viscous dissipation and chemical reaction effects, Int. J. Heat Mass Transf. 55 (2012) 7587–7595.
[27] M.K. Partha, P.V.S.N. Murthy, G.P. Rajasekhar, Effect of viscous dissipation on the mixed convection heat transfer from an exponentially stretching surface, Heat Mass Transf. 41 (2005) 360–366.
[28] M. Sajid, T. Hayat, Influence of thermal radiation on the boundary layer flow due to an exponentially stretching sheet, Int. Commun. Heat Mass Transf. 35 (2008) 347–356.
[29] M.A. Seddeek, Effects of radiation and variable viscosity on a MHD free convection flow past a semi-infinite flat plate with an aligned magnetic field in the case of unsteady flow, Int. J. Heat Mass Transf. 45 (2002) 931–935.
[30] M. Sheikholeslami, S.A. Shehzad, Thermal radiation of ferrofluid in existence of Lorentz forces considering variable viscosity, Int. J. Heat Mass Transf. 109 (2017) 82–92.
[31] C. Zhang, L. Zheng, X. Zhang, G. Chen, MHD flow and radiation heat transfer of nanofluids in porous media with variable surface heat flux and chemical reaction, Appl. Math. Model. 39 (1) (2015) 165–181, https://doi.org/10.1016/j.apm.2014.05.023.
[32] B. Ali, A. Shafiq, I. Siddique, Q. Al-Mdallal, F. Jarad, Significance of suction/injection, gravity modulation, thermal radiation, and magnetohydrodynamic on dynamics of micropolar fluid subject to an inclined sheet via finite element approach, Case Stud. Therm. Eng. 28 (2021) 101537.
[33] S.A. Bakar, N.M. Arifin, N. Bachok, F.M. Ali, Effect of thermal radiation and MHD on hybrid Ag–TiO2/H2O nanofluid past a permeable porous medium with heat generation, Case Stud. Therm. Eng. 28 (2021) 101681.
[34] A.V. Kuznetsov, A.A. Avramenko, Effect of small particles on this stability of bio- convection in a suspension of gyrotactic microorganisms in a layer of finite depth, Int. Commun. Heat Mass Transf. 31 (2004) 1–10.
[35] N.S. Khan, Q. Shah, A. Bhaumik, P. Kumam, P. Thounthong, I. Amiri, Entropy generation in bioconvection nanofluid flow between two stretchable rotating disks, Sci. Rep. 10 (2020) 4448.
[36] A. Shafiq, G. Rasool, C.M. Khalique, S. Aslam, Second grade bioconvective nanofluid flow with buoyancy effect and chemical reaction, Symmetry 12 (2020) 621.
[37] R.R. Kairi, S. Shaw, S. Roy, S. Raut, Thermo-solutal Marangoni impact on bioconvection in suspension of gyrotactic microorganisms over an inclined stretching sheet, J. Heat Transf. 143 (2021) 031201.
[38] S.A.A. Shah, N.A. Ahammad, E.M.T.E. Din, F. Gamaoun, A.U. Awan, B. Ali, Bio-convection effects on Prandtl hybrid nanofluid flow with chemical reaction and motile microorganism over a stretching sheet, Nanomaterials 12 (13) (2022) 2174.
[39] A.U. Awan, S.A.A. Shah, B. Ali, Bio-convection effects on Williamson nanofluid flow with exponential heat source and motile microorganism over a stretching sheet, Chin. J. Phys. 77 (2022) 2795–2810.
[40] S.A.A. Shah, N.A. Ahammad, B. Ali, K. Guedri, A.U. Awan, F. Gamaoun, E.M. Tag-ElDin, Significance of bio-convection, MHD, thermal radiation and activation energy across Prandtl nanofluid flow: a case of stretching cylinder, Int. Commun. Heat Mass Transf. 137 (2022) 106299.
[41] R. Kumar, S. Sood, S.A. Shehzad, M. Sheikholeslami, Numerical modeling of time-dependent bio-convective stagnation flow of a nanofluid in slip regime, Results Phys. 7 (2017) 3325–3332.
[42] M.V. Karwe, Y. Jaluria, Numerical simulation of thermal transport associated with a continuously moving flat sheet in materials processing, J. Heat Transf. 113 (1991) 612–619, https://doi.org/10.1115/1.2910609.
[43] N. Acharya, K. Das, P. Kumar Kundu, Ramification of variable thickness on MHD TiO2 and ag nanofluid flow over a slendering stretching sheet using NDM, Eur. Phys. J. Plus 131 (2016) 303, https://doi.org/10.1140/epjp/i2016-16303-4.
[44] T.S. Neethu, A.S. Sabu, A. Mathew, A. Wakif, S. Areekara, Multiple linear regression on bioconvective MHD hybrid nanofluid flow past an exponential stretching sheet with radiation and dissipation effects, Int. Commun. Heat Mass Transf. 135 (2022) 106115.
[45] D. Pal, S.K. Mondal, MHD Nanofluid bioconvection over an exponentially stretching sheet in the presence of Gyrotactic microorganisms and thermal radiation, BioNanoScience 8 (2018) 272–287, https://doi.org/10.1007/s12668-017-0474-3.
[46] J. Cui, U. Farooq, R. Razzaq, W.A. Khan, M.A. Yousif, Closure to “Computational analysis for mixed convective flows of viscous fluids with nanoparticles” (Farooq, U., Lu, DC, Ahmed, S., and Ramzan, M., 2019, ASME J. Therm. Sci. Eng. Appl., 11 (2), p. 021013), J. Therm. Sci. Eng. Appl. 13 (6) (2021).
[47] A. Mathew, T.S. Neethu, S. Areekara, Three-dimensional hydromagnetic hybrid nanoliquid flow and heat transfer between two vertical porous plates moving in opposite directions: sensitivity analysis, Heat Transf. 50 (2021) 6548–6571, https://doi.org/10.1002/htj.22192.
[48] E.M. Sparrow, H. Quack, C.J. Boerner, Local nonsimilarity boundary-layer solutions, AIAA J. 8 (11) (1970) 1936–1942.
[49] E.M. Sparrow, H.S. Yu, Local non-similarity thermal boundary-layer solutions, J. Heat Transf. 93 (4) (1971) 328–334.
[50] E. Magyari, B. Keller, Heat and mass transfer in the boundary layers on an exponentially stretching continuous surface, J. Phys. D, Appl. Phys. 32 (1999) 577–585, https://doi.org/10.1088/0022-3727/32/5/012.
[51] M. Abd El-Aziz, Viscous dissipation effect on mixed convection flow of a micropolar fluid over an exponentially stretching sheet, Can. J. Phys. 87 (2009) 359–368, https://doi.org/10.1139/P09-047.